ACS OMEGA

http://pubs.acs.org/journal/acsodf

Article

Effect of Sizing Agents on Surface Properties of Carbon Fibers and Interfacial Adhesion of Carbon Fiber/Bismaleimide Composites

Tian Yang, Yan Zhao,* Hansong Liu, Mingchen Sun, and Shu Xiong

Cite This: *ACS Omega* 2021, 6, 23028−23037

Read Online

ACCESS | Metrics & More | Article Recommendations | Supporting Information

ABSTRACT: Physicochemical, surface, and mechanical properties of three batches of T800 grade carbon fibers (CFs) treated with three kinds of sizing agents and Toray T800H CFs were characterized to study the effect of sizing agents on surface properties. Scanning electron microscopy for morphology, atomic force microscopy calculations, and results for the content of sizing agents showed that sizing agent B improved the surface roughness and CFs with high content of sizing agent always presented small surface roughness in a certain content range 1.2−1.6%. Surface energy of CFs was calculated by Young's contact angle using the test results with water and glycol, and contact angles with LY-1 and modified-AC531 were also acquired. The results proved that CFs of sizing agent group B had the highest average surface energy and the lowest average contact angles with both LY-1 and modified-AC531. From both single-filament and tensile strength test results, the average strength of CFs of sizing agent group B was found to be the lowest, which indicated that sizing agent B had an influence on tensile strength decrease of T800 grade CFs. Comparing the results of interfacial shear strength both in a natural dry state and after hygrothermal treatment, high surface energy was found to be the key element to obtain high interfacial adhesion between T800 grade CFs and bismaleimide, and high surface roughness and low contact angle also played important roles. Among sizing agents A, B, and C, A had an effect on the interfacial shear strength decrease of CFs in the natural dry state, while C had that after hygrothermal treatment.

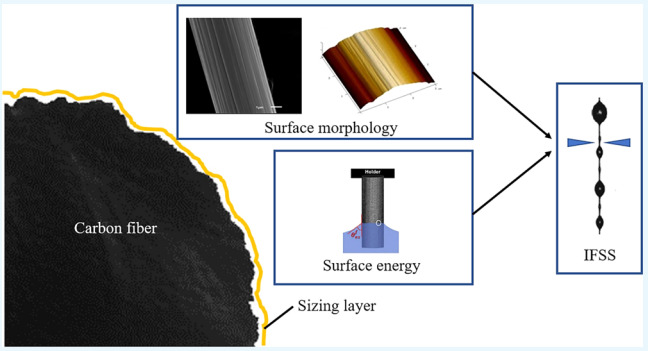

1. INTRODUCTION

Carbon fibers (CFs) are considered as important reinforcements, which are widely used in advanced resin matrix composites. To achieve high strength CF composites, mechanical properties of CFs and bonding performance between CFs and the matrix are two essential factors when resin matrix is fixed. Mechanical properties of CFs are mainly determined by the internal structure, such as compactness, crystallinity, and defects, while bonding performance is normally relevant to CF surface properties. As sizing agents often play a great role in improving CF surface properties, it is meaningful to investigate the effect of sizing agents on surface properties of CFs. Researching results can effectively guide CF manufacturers to optimize the production process.[1−3]

CFs with characteristic strength higher than 5.5 GPa and modulus between 290 and 300 GPa are generally considered as T800 grade CFs. T800 grade CFs improve the mechanical performance of CF-reinforced composites and great progress on the research on T800 grade CFs in China has been achieved with the establishment of T800 grade CF production line.[4−6]

Compared with epoxy resin, bismaleimide (BMI) resin is a kind of thermosetting resin with better thermal stability, and its glass transition temperature is higher than 250 °C.[7−11] By blending with inorganic fillers or bisphenol A, the thermal aging property of BMI resin can be further improved.[12−15] In addition, BMI resin also has other excellent characteristics such as dielectric properties, friction resistance, and lightning resistance.[9] These properties make CF/BMI composites suitable for extremely harsh conditions such as high-temperature environments.[16−22]

Interfacial adhesion properties between T800 grade CFs and BMI matrix determine the competence of load transfer from the matrix to CFs.[23−26] CF surface, resin matrix, and sizing agents are involved in the formation of interfacial adhesion. The mechanisms of interfacial adhesion of composites mainly include diffusion entanglement,[27−29] chemical bond,[30] electrostatic attraction,[31−33] and mechanical engagement.[34,35] The usage of sizing agents in commercial CF manufacturing is proved successfully to protect CF surface, enhance surface

Received: March 1, 2021
Accepted: May 14, 2021
Published: September 1, 2021

properties, and take full advantage of those adhesion mechanisms. Wu et al.[36] studied the effect of sizing on interfacial adhesion of commercial CF (T700SC) with BMI composites, and results indicated that the EP-type sizing agents tended to lead to stronger interfacial adhesion, but this trend was not obvious. However, for T800 grade CFs and BMI resin, there is a lack of research on the effect of sizing agents on interfacial properties of CF/BMI composites. Thus, investigation of the effect of sizing agents on interfacial adhesion of CF/BMI composites is useful in the design and manufacture of CF/BMI components and parts.

In order to get a better understanding of the effect of sizing agents on surface properties and interfacial adhesion, physicochemical, surface, and mechanical properties of three batches T800 grade CFs treated by three kinds of sizing agents and Toray T800H CF were characterized. Linear density, volume density, sizing agent content, and monofilament and multifilament tensile properties of CFs were obtained by common methods. Scanning electron microscopy (SEM) for morphology and atomic force microscopy (AFM) were conducted to acquire surface morphology and roughness. Surface energy was tested by Wilhelmy hanging method,[37] and interface shear strength of CF/BMI composites was tested by the micro-debonding method[38] with both no treatment and a certain period of hydrothermal treatment.[39,40]

2. MATERIALS AND METHODS

2.1. Raw Materials. CFs used in this work were nine kinds of T800 grade CFs (12K) from AVIC Composite Corporation and T800H CF (12K) from Toray Industries. A, B, and C represent three types of sizing agents. M1, M4, and M5 represent the first, fourth, and fifth batch of T800 grade CF. Three batches of CFs were manufactured by the same process, except different sizing agents in the sizing process. BMI resin (AC631) was obtained from AVIC Composite Corporation. The solvent ethyl alcohol was purchased from Beijing Chemical Works. All reagents were of analytical grade.

2.2. Physicochemical Characterizations of CFs. The CF samples covered with filter paper were sent to a Soxhlet extractor. Acetone (300 mL) was added to the flask as the solvent. The CF samples were extracted at 125 °C for 2 h (refluxed at least 8 times) to remove sizing agents. Then the samples were dried in an infrared oven at 105 ± 5 °C to remove solvents.

Surface morphology of CFs was observed using a cold field scanning electron microscope (HITACHI JSM-7500) with an acceleration voltage of 20 kV. AFM (Veeco D3000) was used to further observe the surface morphology. The scanning area was selected as 3 μm × 3 μm. Based on the observation of AFM, a software Nano Scope was used to calculate the maximum and arithmetic average surface roughness. For sized CFs, Fourier transform infrared (FTIR) spectroscopy measurements were performed using Nicolet 6700 FTIR spectrometer.

2.3. Surface Energy of CFs. Contact angles were characterized by DCTA21 Surface/interface tensiometer. Wilhelmy hanging method was used to measure the advancing contact angle between CFs and two types of testing liquid. The average result of three tests was chosen as the contact angle between each liquid and CFs.

The surface energy of CFs was calculated by Young's contact angle. In order to decrease the error caused by the dispersion of monofilaments, four CF monofilaments were stuck to a round clamp, parallel with each other and vertical to the bottom of the clamp, to ensure that all CF monofilaments touched the testing liquid at the same time.

Contact angles between the CFs and LY-1 and modified-AC531 resin system were also acquired. The tests were conducted at the room temperature of 25 °C, and the surface tensions of the two resin systems were obtained every 5 °C.

2.4. Tensile Test of CF Single Filament and CFs. Single-filament tensile test of CFs was carried out by Instron 5967 configured and 5N sensor in accordance with ASTM D3379. When preparing the sample, CFs were divided into filaments, and filaments with a length of about 25 mm were selected. The selected filaments were stuck to the testing paper frame of 20 mm. The breaking strength and the percentage of breaking elongation of a single filament were calculated by displacements and tension recorded during the test.

The tensile test of CFs was done in accordance with GB/T 26749 by the Instron 5967 universal mechanical testing machine. An extensometer with a 50 mm span supplied by Instron was used for the modulus test. The load−displacement curve was recorded during the test.

2.5. Interfacial Shear Strength of CF/BMI Composites. The micro-debonding test was carried out by a self-developed instrument. The monofilament was stuck on a self-made C-shaped frame by double-sided tape. Resin and curing agent were mixed in a certain proportion and were applied to the fixed monofilament using a pin. The monofilament with resin microsphere was sent to an oven and cured. The cured monofilament composite was fixed on a self-made concave sample clamp. Special glue was used to fix the monofilament further. The sample clamp was placed on the micro-debonding instrument, and the resin microsphere was aligned under the observation of an optical microscope. After the size of the microsphere was measured, force−time curve during the exfoliation process was recorded. The maximum force on the curve was regarded as the exfoliating force on the resin microsphere.

The hygrothermal state samples were obtained as follows: enough micro-debonding samples (at least 10 per group) were prepared and placed into a damp-heat test chamber. The environment temperature was set to 70 °C, and it was ensured that the temperature error was within ±3 °C. The test piece was immersed in a beaker of water. The beaker was placed into the chamber and the boiling method was used to adjust the moisture absorption state of the test piece for 7 days. After adjusting the hygrothermal state of samples, the beaker was taken out and samples were removed. Then, the micro-debonding test was conducted at room temperature immediately.

3. RESULTS AND DISCUSSION

3.1. Physicochemical Properties of CFs. The contents of sizing agents are shown in Table 1. Among these CFs, M4-A presented the highest content of sizing agent, which was 1.60%. The lowest content of the sizing agent was 0.80%, from both M4-C and M5-C. CFs of sizing agent group C exhibited the lowest average content among groups A, B, and C, which indicated that sizing agent C had weaker bonding to CFs. Comparing the content of CF batch M1, M4, and M5, M5 showed the lowest content in each sizing agent group, which meant that M5 CFs had weaker bonding to the sizing agent. The sizing agent contents of group A and group B were both higher than that of Toray T800H, while that for the C group was not.

https://doi.org/10.1021/acsomega.1c01103
ACS Omega 2021, 6, 23028−23037

Table 1. Contents of Sizing Agents of CFs

CF	contents of sizing agents (%)
M1-A	1.37
M4-A	1.60
M5-A	1.20
M1-B	1.51
M4-B	1.40
M5-B	1.30
M1-C	1.10
M4-C	0.80
M5-C	0.80
T800H	1.10

FTIR spectra of 10 kinds of CFs are presented in Figure 1. The chemical structures of the 10 kinds of CFs were similar. It

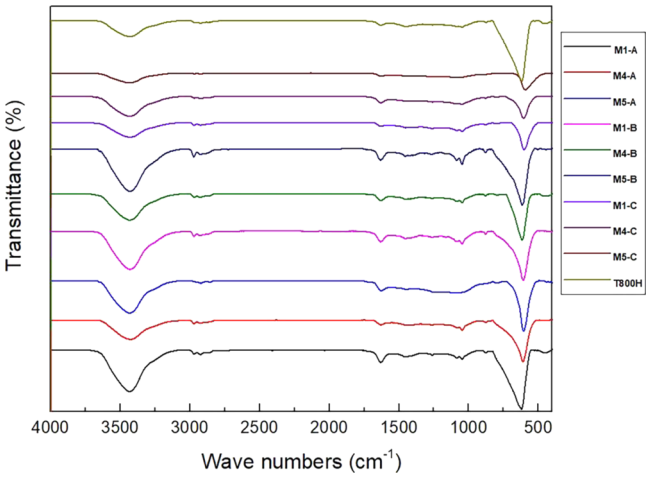

Figure 1. FTIR spectra of 10 kinds of CFs.

indicated that the spectrum of fiber-sizing agents confirmed the presence of epoxy (915 cm^{-1}), hydroxyl (3430 cm^{-1}), ether (1047 cm^{-1}), and benzene (1632 cm^{-1}). Furthermore, the vibrations of C−H of para-benzene (792 cm^{-1}) and of -CH2- (1453 and 2970 cm^{-1}) suggest that the sizing agents mainly consisted of diglycidyl ether of bisphenol A-type epoxy constituent, which will influence the chemical properties of the 10 kinds of CFs. In this research, from FTIR results, there existed no obvious difference of curves of the 10 kinds of sizing agents, and it can be concluded that the chemical structure of several sizing agents contained epoxy. For CF/BMI composites, the chemical bonding of these sizing agents and matrix had no obvious distinction.

The linear density and volume density results of the 10 CFs are shown in Table 2. The linear density values of M5 batch CFs ranged from 442 g/km to 453 g/km, which indicated that the manufacturing quality of the M5 batch CF was not as good as that of M1 (439−442 g/km) and M4 (445−448 g/km). The volume densities of nine kinds of T800 grade CFs were 1.76−1.78 g/cm3 without significant difference. Comparing nine kinds of T800 grade CFs and Toray T800H, Toray T800H had lower linear density and higher volume density, which indicated that Toray T800H had a lower fiber diameter than the other T800 grade CFs.

3.2. Surface Morphology of CFs. Different cross-section shapes of CFs were observed by SEM, as shown in Figure 2a (M1-A) and Figures S1 and S2 (Supporting Information). M1-

Table 2. Linear Density and Volume Density Values of 10 Kinds of CFs

CF	linear density (g/km)	volume density (g/cm^3)
M1-A	442	1.76
M4-A	445	1.78
M5-A	453	1.76
M1-B	441	1.78
M4-B	448	1.78
M5-B	442	1.77
M1-C	439	1.78
M4-C	445	1.77
M5-C	448	1.76
T800H	436	1.79

B, M5-B, M4-C, and M5-C present a circular cross section, while M1-A, M1-C, M4-A, M4-B, and Toray T800H present a flat ellipse cross section. M5-A had a typical "cashew" shape, and this could be the reason that M5-A had the lowest content of sizing agent among M1-A, M4-A, and M5-A.

As seen from Figure 2b, obvious grooves were distributed along the fiber direction on the surface of all 10 CFs. The surface grooves of nine T800 grade CFs were similar to those of Toray T800H. There were small "particles" on the surface of M5-B, which was speculated to be caused by uneven coating of sizing agents, considering its low sizing agent content among M1-B, M4-B, and M5-B. Normally, the surface of wet spinning pro-filaments contains distributing grooves. In CF formation process of wet spinning, axial elongation and radial shrinkage of fibers happen at the same time. During filament densification, the cross section of filament gradually decreases imbalance, causing the formation of surface-folded wrinkles. Therefore, the side surface morphology proved that these T800 grade CFs were manufactured using the wet spinning method.

As shown in Figure 3 (M1-A) and Figure S3 (Supporting Information), all CFs had grooves along the axial direction on the surface, and the morphologies of "ridge" and "valley" were clearly found. M1-A, M1-B, M1-C, and M5-C had larger numbers of "ridges" and "valleys" than the others, while their widths were relatively small. M4-A, M5-A, M4-B, M4-C, M5-B, and Toray T800H had larger grooves, especially in width. Among these 10 CFs, grooves of M1-B were relatively shallow, which was beneficial for sizing agents filling the grooves. Thus, it could be explained that the sizing agent content of M1-B is the highest in sizing agent group B.

The results in Table 3 showed that M5-A had the largest average surface roughness (32.53 nm), while M1-B had the smallest roughness (19.15 nm). It proved that M1-B had a smoother surface than the others. This point was in compliance with the conclusion that M1-B had shallow relative grooves among all CFs in Figure S3 (Supporting Information).

Every CF in sizing agent group B had the smallest average surface roughness in its CF batch group. For example, the average surface roughness of M1-B was 19.15 nm, which was the smallest one in the M1 batch. Thus, it was concluded that the sizing agent could influence the surface roughness of CFs. Comparing sizing agent group A, B, and C, group B had a good effect on surface roughness improvement. For every batch of CFs, the average roughness of the M4 batch ranged from 21.38 to 23.08 nm, while the M1 batch and M5 batch ranged from 19.15 to 29.48 nm and from 23.91 to 32.53 nm, respectively. This indicated that the manufacturing quality of M4 batch CFs

https://doi.org/10.1021/acsomega.1c01103
ACS Omega 2021, 6, 23028−23037

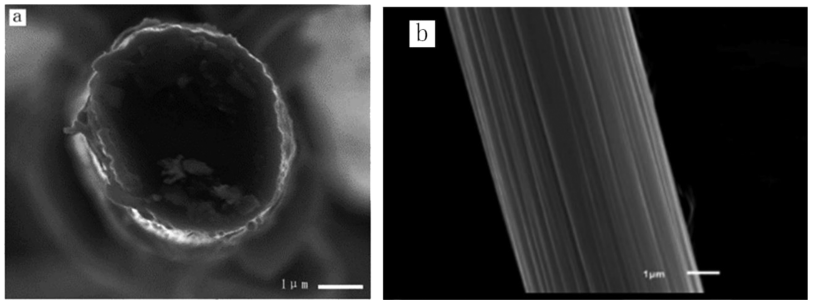

Figure 2. SEM image of CF M1-A (a) cross-section shapes and (b) lateral surface.

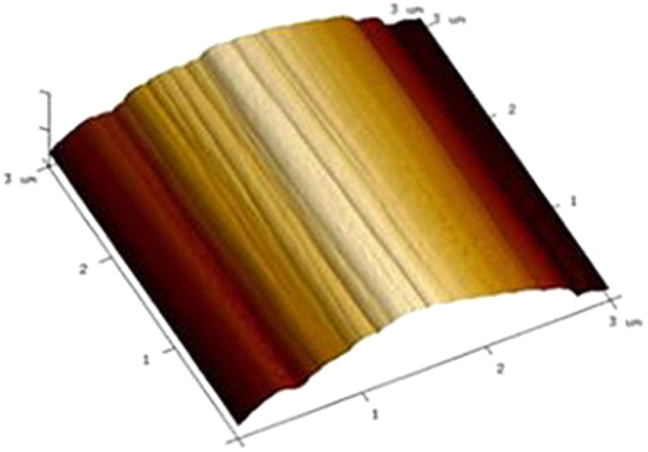

Figure 3. AFM morphologies of CF M1-A.

Table 3. Surface Roughness of CFs

CF	$\bar{R}a$ (nm)	Ra_{max} (nm)
M1-A	28.50	238
M4-A	22.43	163
M5-A	32.53	231
M1-B	19.15	176
M4-B	21.38	228
M5-B	23.91	285
M1-C	29.48	189
M4-C	23.08	184
M5-C	26.02	230
T800H	26.77	290

was controlled well. M4-B showed the lowest average roughness in the M4 batch, which proved again that sizing agent B had a good effect on roughness improvement.

Considering the relationship between the sizing agent content and surface average roughness, it was found that CF with a high content of sizing agent always presented small surface roughness in a certain content range 1.2−1.6%. Sizing agent groups A and B happened in accordance with this point. For example, M4-A had the highest content and the surface roughness was the lowest in group A.

Similar conclusions were not found from the results of maximum roughness, and there was no meaningful relationship between average roughness and maximum roughness or between sizing agent content and maximum roughness. M1-A, M5-A, M4-B, M5-B, and M5-C had larger maximum roughness than the others. The roughness of M5-B (285 nm) was the largest among nine kinds of T800 grade CFs, while that of Toray T800H (290 nm) was higher than that of M5-B.

3.3. Wettability and Surface Energy of CFs. Surface wettability is one of the key properties in the process of prepregs and composites processing. A large number of active functional groups contained in sizing agents are expected to improve the surface wettability of CFs. In this research, a dynamic contact angle test was used to characterize the surface wettability. The aim of dynamic contact angle measurement was to obtain the wetting force F of resin on CFs, and then calculate the contact angle between resin and CFs according to Young's equation.

$$F = P\gamma \cos\theta \tag{1}$$

In formula (1), F is the force induced by the instrument; P is the wetting perimeter of testing monofilament; and γ is the surface tension of testing liquid. According to OWRK equation, the surface energy of CF under specific testing liquid can be obtained using eq 2.

$$\gamma_L(1 + \cos\theta) = 2\sqrt{\gamma_L^d \gamma_s^d} + 2\sqrt{\gamma_L^p \gamma_s^p} \tag{2}$$

In formula (2), γ_L is the surface energy of the testing liquid, γ_L^d is testing liquid dispersion component, γ_L^p is the polar component of testing liquid, γ_s^d is the solid dispersion component, and γ_s^p is the polar component of the solid. θ is the contact angle formed by testing liquid on the solid surface.

Two small molecular liquids (water and ethylene glycol) with medium and high surface tension and polarity components were selected as detection liquids. The ideal values of surface tension and polarity/dispersion components of the two testing liquids at room temperature are shown in Table 4.

Table 4. Surface Tension and Its Polarity and Dispersion Components of the Infiltration Fluid

liquid	surface tension γ_L (mN·m−1)	dispersion component γ_L^d (mN·m−1)	polar component γ_L^p (mN·m−1)	surface polarity parameter <keep-together>γ_L^p/γ_L</keep-together>
water	72.75	22.10	50.65	0.70
ethylene glycol	48.00	29.00	19.00	0.40

According to the similarity compatibility principle, in the process of preparing composites, large surface energy ensures that CFs can be infiltrated easily by a matrix such as epoxy, and it further improves the bonding between CFs and the matrix.

Results in Figure 4 showed that the contact angles of M4-A, M1-B, M4-B, and M5-C with water were fairly small (under 62) and those of M4-A, M5-B, M1-C, and M5-C with glycol were relatively small (under 50). The numeric ranges of

https://doi.org/10.1021/acsomega.1c01103
ACS Omega 2021, 6, 23028−23037

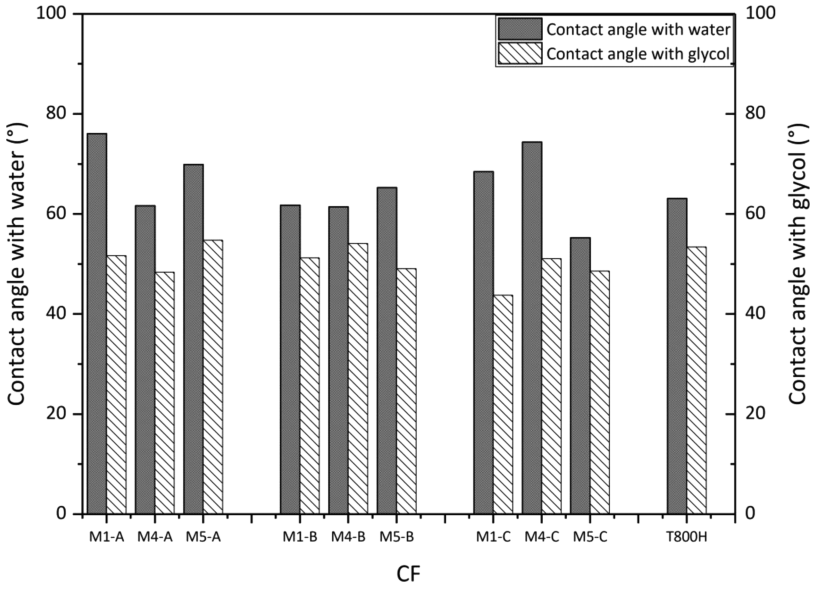

Figure 4. Contact angle between CFs and the wetting fluid.

contact angles of every sizing agent group were 61.64−76.03(A), 61.44−65.26(B), and 55.25−74.34(C) with water and 48.34−54.74(A), 49.09−54.13(B), and 43.74−51.09(C) with glycol. The numeric ranges of contact angle of sizing agent group B with both water and glycol were narrower than those of both groups A and C, which indicated that the quality of sizing agent B was stable when sizing to T800 grade CFs. Contact angles of Toray T800H with water and glycol were included in the numeric ranges of sizing agents A and B, while sizing agent C and sizing agent of Toray T800H were quite different from the wettability of glycol. As different sizing agents had quite different numeric ranges of contact angles, it proved that sizing agents could influence the wettability of CFs.

As seen from Figure 5, M5-C had the largest surface energy of 48.84 mJ·m^{-2}, while M1-A had the smallest surface energy of 31.57 mJ·m^{-2}. The surface energies of M1-B, M4-B, M4-A, and T800H were relatively large. The larger surface energy of the CF surface is considered as the contribution of better dispersive and more active polar components. These two factors are beneficial for adhesion between resin and CFs. Sizing agent group B had the highest average surface energy among groups A (34.68), B (39.66), and C (38.81). The contact angles with glycol of these 10 kinds of CFs were slightly different, and there was a tight correspondence between the contact angle with water and the surface energy. For CF/BMI composites usage, a high contact angle with water of CF related to high surface energy. For example, the contact angle with water of M5-C was the highest among the 10 kinds of CFs, and the surface energy was also the highest.

Surface tension of LY-1 and modified-AC531 resin were tested at different temperatures. From the results in Figure 6, surface tension of LY-1 was slightly larger than that of modified-AC531.

Contact angles between 10 kinds of CFs and two resin systems are shown in Figure 7. Except M4-B, the contact

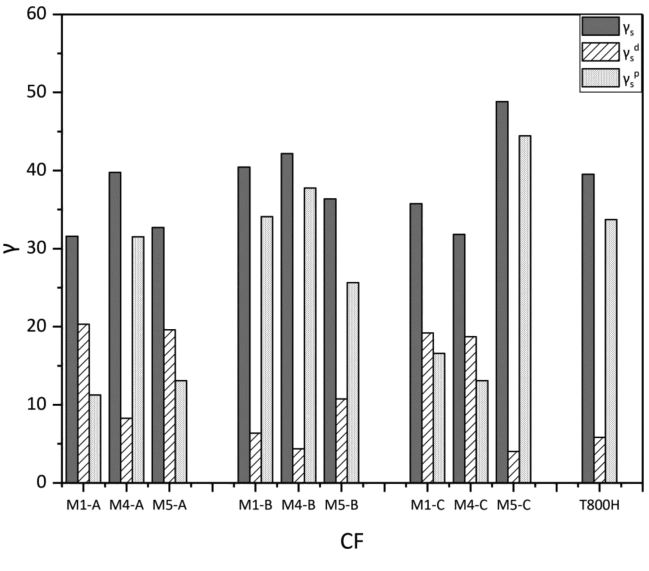

Figure 5. Surface energy of CFs.

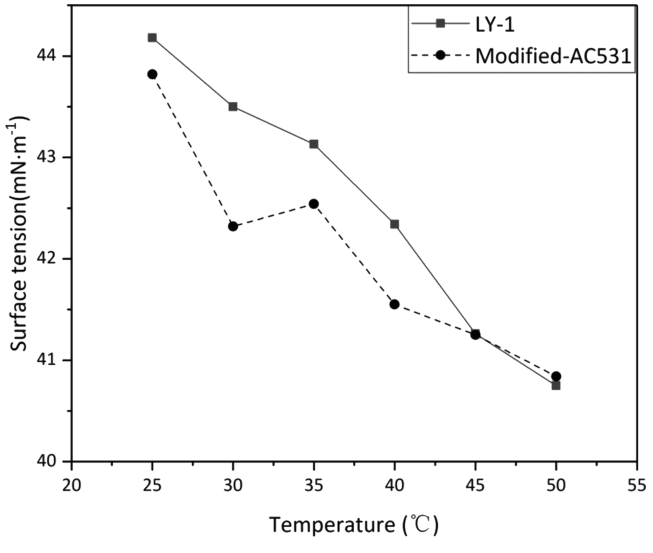

Figure 6. Surface tension of two resin systems at different temperatures.

https://doi.org/10.1021/acsomega.1c01103
ACS Omega 2021, 6, 23028−23037

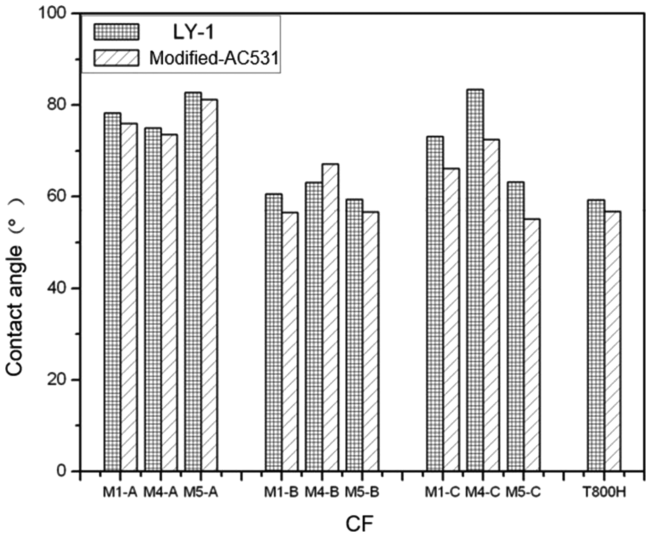

Figure 7. Contact angles between CFs and different resin.

angles of the modified-AC531 resin system with CF were smaller than that of LY-1, which indicated that CF infiltrated in modified-AC531 resin better than LY-1. Sizing agent group B had the lowest average contact angles among groups A, B, and C with both LY-1 and modified-AC531, which indicated that sizing agent B improved wettability of T800 grade CF surface. Comparing the results, CFs with smaller contact angles with LY-1 resin were M1-B, M4-B, and M5-B, and CFs with smaller contact angles with modified-AC531 resin were M1-B, M5-B, and M5-C. Hence, the large surface energy CFs in Figure 5 were roughly consistent with the CFs with smaller contact angles in Figure 6, which proved that a suitable kind of sizing agent could improve the surface energy of CFs and further improve the contact angles between CFs and resin. Considering Toray T800H, it presented small contact angles with both LY-1 and modified-AC531, which was closer to sizing agent group B than those for groups A and C.

3.4. Mechanical Properties of CFs. Tensile strength of CFs is affected by randomly distributing surface and internal defects but determined by the biggest defect, according to the weakest connection theory. Weibull's weakest connection theory was selected to study the dispersion of tensile strength of CFs. The two-dimensional Weibull distribution equation describing the tensile strength of CF is shown in eq 3

$$P_f(\sigma, l) = 1 - \exp[-(l/l_0)(\sigma/\sigma_0)^m] \quad (3)$$

where σ_0 is the Weibull dimension parameter of CF strength with the physical meaning of breaking strength of fiber with a length of l_0. m is the shape parameter to represent the dispersion of fiber strength. All T800 grade CFs measured in the test were of length 20 mm. The reference length l_0 was chosen as 20, and the formula changed to the following formula.

$$P_f(\sigma, l) = 1 - \exp[-(\sigma/\sigma_0)^m] \quad (4)$$

Sequence of the breaking strength σ_i from small to large, i = 1, 2, 3.....N; N is the total number of fibers measured. The probability of fracture under i is P_i.

$$P_i = \frac{n - 0.5}{N} \quad (5)$$

Formula (5) is simplified to the following formula

$$\ln[-\ln(1 - P)] = m \ln \sigma - m \ln \sigma_0 \quad (6)$$

The slope of the curves of $\ln[-\ln(1 - P)]$ and $\ln \sigma$ is m, and $\ln \sigma_0$ can be obtained through the intercept. According to the expected value formula of Weibull distribution, the average breaking strength of CFs can be obtained.

$$\bar{\sigma} = \sigma_0 \Gamma\left(1 + \frac{1}{m}\right) \quad (7)$$

Figure 8 shows the fitting curves of the strength test data of 10 CF single filaments according to eq 6. The fitting results of strength test data are shown in Table 5. Among the fitting curve R values, M5-B was the lowest. It can be explained as M5-B being affected by the larger random length of defects than the other CFs as M5-B (285 nm) showed the largest maximum roughness among nine kinds of T800 grade CFs. Comparing the average R values of sizing agent groups A, B, and C, group B was the lowest, indicating that sizing agent B reduced the consistency of CFs. The average fracture strength was in the range of 4320−5023 MPa and that of T800H was 4735.20 MPa. The average strengths of CF batches were fairly close, which were 4749 MPa (M1 batch), 4717 MPa (M4 batch), and 4806 MPa (M5 batch). Average strengths of CFs with sizing agent groups were 4842 MPa (A group), 4503 MPa (B group), and 4926 MPa (C group) and that of sizing agent group B was obviously low, which indicated that sizing agent B had an effect on the strength decrease of T800 grade CF single filament.

The tensile strength of CF is normally determined by means of gluing, curing, and stretching of CF bundles. The results of tensile strength of 10 CFs are shown in Table 6. The tensile strength was in the range of 5336−6038 MPa and that of T800H was 5612 MPa. The average tensile strengths of CF batches were 5473 MPa (M1 batch), 5710 MPa (M4 batch), and 5636 MPa (M5 batch), while those of sizing agent groups were 5559 MPa (A group), 5417 MPa (B group), and 5844 MPa (C group). The average tensile strength of sizing agent group B was obviously lower than those of groups A and C, which further proved that sizing agent B had an effect on the tensile strength decrease of CFs. The tensile strength values of M5-B, M4-B, and M1-B were 5477.82 MPa, 5437.52 MPa, and 5335.77 MPa, respectively, which excluded the possibility of an abnormal M5-B sample for tensile strength decrease.

3.5. Interfacial Shear Strength. In order to study the effect of sizing agent on interfacial adhesion of CF/BMI composites, interfacial shear strength of CF/AC631 BMI composite was tested in both a natural dry state and hygrothermal treatment state. As shown in Table 7, the average interfacial shear strengths of CF batches in the natural dry state were 74.42 MPa (M1 batch), 70.95 MPa (M4 batch), and 75.52 MPa (M5 batch), while those of sizing agent groups were 71.29 MPa (A group), 74.79 MPa (B group), and 74.81 MPa (C group). The average interfacial shear strength of the CF M4 batch was obviously lower than those of the M1 and M5 groups, which indicated that the interfacial properties between M4 CFs and sizing agents were not as good as those of M1 and M5 CFs. The average interfacial shear strength of sizing agent group A was obviously lower than those of group B and group C, which indicated that sizing agent A had an effect on the decrease of CFs in the natural dry state.

On synthesizing the relevant results, it was found that the surface energy of CFs was the key element to determine the interfacial shear strength in the natural dry state. For example,

https://doi.org/10.1021/acsomega.1c01103
ACS Omega 2021, 6, 23028−23037

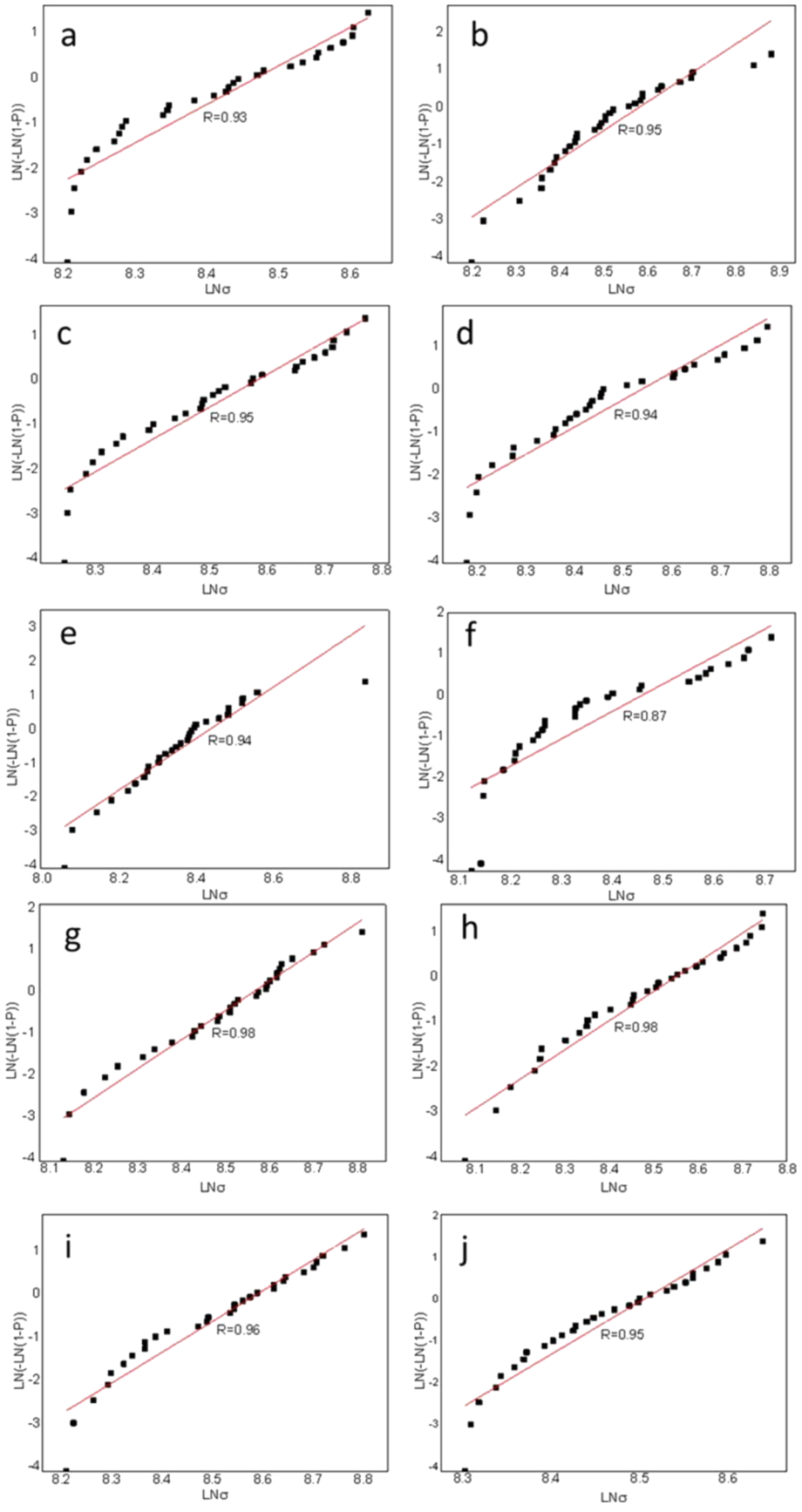

Figure 8. Fitting curves of strength data of 10 kinds of CF single filament: (a) M1-A; (b) M4-A; (c) M5-A; (d) M1-B; (e) M4-B; (f) M5-B; (g) M1-C; (h) M4-C; (i) M5-C; and (j) T800H.

https://doi.org/10.1021/acsomega.1c01103
ACS Omega 2021, 6, 23028−23037

Table 5. Tensile Strength of 10 Kinds of CF Single-Filament

CF	m	R	$\bar{\sigma}$ (MPa)
M1-A	8.48	0.93	4518.51
M4-A	7.69	0.95	5011.52
M5-A	7.30	0.95	4995.96
M1-B	6.36	0.94	4791.32
M4-B	7.59	0.94	4320.14
M5-B	6.66	0.87	4398.91
M1-C	7.01	0.98	4936.51
M4-C	6.49	0.98	4818.72
M5-C	7.14	0.96	5023.21
T800H	12.58	0.95	4735.20

Table 6. Tensile Strength of CFs

CF	the tensile strength (MPa)	increased percentage relative to T800H (%)	coefficient of dispersion (%)
M1-A	5519.10	−1.66	6.95
M4-A	5656.98	+0.80	4.14
M5-A	5501.45	−1.97	2.03
M1-B	5335.77	−4.92	2.78
M4-B	5437.52	−3.11	3.81
M5-B	5477.82	−2.39	4.76
M1-C	5566.52	−0.81	2.81
M4-C	6037.61	+7.58	4.09
M5-C	5930.55	+5.68	2.03
T800H	5612.00	0.00	3.70

Table 7. Interfacial Shear Strength of CF/AC631 Composites

	natural dry state		after hygrothermal treatment		
CF	IFSS (MPa)	CV (%)	IFSS (MPa)	CV (%)	IFSS retention rate (%)
M1-A	73.12	10.96	52.10	10.40	71.25
M4-A	68.39	4.71	48.45	9.19	70.84
M5-A	72.36	8.91	49.75	7.78	68.75
M1-B	74.20	7.90	53.65	9.18	72.30
M4-B	79.91	5.40	51.93	11.02	64.99
M5-B	70.25	10.58	49.97	11.17	71.13
M1-C	75.93	0.70	41.81	0.48	55.06
M4-C	64.54	9.57	49.74	10.07	77.07
M5-C	83.96	5.56	56.49	13.67	67.28
T800H	74.56	15.96	51.61	5.47	69.22

high interfacial shear strength CFs such as M5-C, M4-B, and M1-C were all high in surface energy, while CFs with low surface energy such as M1-A, M5-A, and M4-C could not exceed the medium level of interfacial shear strength. Except surface energy, high surface roughness, and low contact angle with modified-AC531 were also important for interfacial shear strength improvement. For example, M1-A and M5-A had low surface energy but high surface roughness, and their interfacial shear strength turned out to be in the middle level. Comparing M1-A, M5-A, and M4-C, M4-C had a relatively low surface roughness and its interfacial shear strength was the lowest. Comparing M4-A and M1-B, their surface energies were quite close and the roughness of M4-A was higher, but the interfacial shear strength of M4-A was much lower than that of M1-B. It was because the contact angle with modified-AC531 of M1-B was much lower than that of M4-A. Further explanation was that during the processing of composites, M1-B had better infiltration and better bonding with resin matrix than M4-A.

3.6. Interfacial Shear Strength after Hygrothermal Treatment. The interfacial shear strength of CF/AC631 composites after hygrothermal treatment are shown in Table 7. Like the result in the natural dry state, M5-C was consistent with the highest strength. The interfacial shear strengths of M4-A and M4-C were low whether in the natural dry state or after hygrothermal treatment. The surface energies of M5-C, M4-B, and M1-B were fairly high among these 10 kinds of CFs, while the interfacial shear strengths after hygrothermal treatment were also relatively high. Thus, it was also concluded that the surface energy was the key element to determine the interfacial shear strength after hygrothermal treatment. The average interfacial shear strengths of CF batches after hygrothermal treatment were 49.19 MPa (M1 batch), 50.04 MPa (M4 batch), and 52.07 MPa (M5 batch), while those of sizing agent groups were 50.10 MPa (A group), 51.85 MPa (B group), and 49.35 MPa (C group). The average interfacial shear strength of group C was obviously lower than that of groups A and B, which indicated that sizing agent C had an effect on the decrease after hygrothermal treatment.

The interfacial shear strength in the natural dry state and after hygrothermal treatment were substituted into the following formula to calculate the retention rate

$$\eta = \frac{\tau_d}{\tau_w} \times 100\% \tag{8}$$

where η is the interfacial shear strength retention rate, %; τ_d is the interfacial shear strength at the natural dry state, MPa; and τ_w is the interfacial shear strength after hygrothermal treatment, MPa.

From Table 7, it can be seen that the retention rate ranged from 55.06 to 77.07% and that of Toray T800H was 69.22%. M4-C had the highest retention rate (77.07%), while M1-C had the lowest interfacial shear strength retention rate (55.06%). The retention rates of sizing agent groups were 70.3% (A group), 69.5% (B group), and 66.5 (C group). The retention rate of sizing agent group C was obviously low which pointed out again that sizing agent C reduced the interfacial adhesion.

4. CONCLUSIONS

(1) SEM morphology showed that the profile of T800 grade CFs was "flat ellipse" or "circular", while M5-A had a "waist" shape, which might cause a low content of sizing agents. In both SEM and AFM results, obvious grooves were distributed along the axial direction on the surface. The AFM morphology showed that the grooves on the M1-B surface were shallow among all CFs.

(2) Sizing agents had an influence on the surface average roughness of CFs. Comparing sizing agents A, B, and C, sizing agent B had an effect on surface roughness improvement of T800 grade CFs. The surface roughness of M1-B was the smallest among all CFs, in compliance with the observation of AFM morphology. It was also found that in a certain content range 1.2−1.6%, CFs with higher content of sizing agent had smaller surface roughness normally. There was no meaningful relationship between average roughness and maximum roughness or between sizing agent content and maximum roughness.

https://doi.org/10.1021/acsomega.1c01103
ACS Omega 2021, 6, 23028−23037

(3) As different sizing agent groups had quite different numeric contact angle range, it showed that sizing agents had an effect on the wettability of CFs. The numeric ranges of contact angle of sizing agent group B with both water and glycol were narrower than those of both groups A and C. The contact angles with glycol of these 10 kinds of CFs were slightly different, and there was a tight correspondence between the contact angle with water and the surface energy. M5-C was found to have the highest contact angle with water and surface energy among the 10 kinds of CFs. Sizing agent group B had the highest average surface energy among groups A (34.68), B (39.66), and C (38.81). Meanwhile, group B had the smallest average contact angles with both LY-1 and modified-AC531, which proved that sizing agent B improved the wettability of the CF surface. Toray T800H presented small contact angles with both LY-1 and modified-AC531, which was closer to that of sizing agent group B than those of groups A and C. Generally, T800 grade CF with high surface energy had small contact angles with modified-AC531.

(4) From single-filament test results, it could be found that average tensile strength values of CF batches (M1, M4, M5) were fairly close, while that of sizing agent group B was obviously lower than those of group A and C. The strength decrease phenomenon of T800 grade CF single filament caused by sizing agent B indicated that sizing agent B reduced the consistency of CFs and further decreased single filament strength. Considering the tensile strength of CFs, the sizing agent group B (5417 MPa) was obviously lower than group A (5559 MPa) and C (5844 MPa), which indicated that sizing agent B had an effect on the tensile strength decrease of CFs. This was in accordance with the conclusion obtained from the single filament test.

(5) The surface energy of T800 grade CFs was the key element to determine the interfacial shear strength. High surface energy, high surface roughness, and low contact angle with resin matrix were beneficial for high interfacial shear strength in the natural dry state. Sizing agent A had an effect on the strength decrease of CFs in the natural dry state, while sizing agent C had that after hygrothermal treatment.

■ ASSOCIATED CONTENT

Supporting Information

The Supporting Information is available free of charge at https://pubs.acs.org/doi/10.1021/acsomega.1c01103.

SEM image of CF cross-section shapes and lateral surface and AFM morphologies of CFs (PDF)

■ AUTHOR INFORMATION

Corresponding Author

Yan Zhao − *School of Materials Science and Engineering, Beihang University, Beijing 100191, China;* orcid.org/0000-0001-7776-2415; Email: jennyzhaoyan@buaa.edu.cn

Authors

Tian Yang − *School of Materials Science and Engineering, Beihang University, Beijing 100191, China*

Hansong Liu − *School of Materials Science and Engineering, Beihang University, Beijing 100191, China*

Mingchen Sun − *School of Materials Science and Engineering, Beihang University, Beijing 100191, China*

Shu Xiong − *School of Materials Science and Engineering, Beihang University, Beijing 100191, China*

Complete contact information is available at: https://pubs.acs.org/10.1021/acsomega.1c01103

Author Contributions

Conceptualization, T.Y. and Y.Z.; methodology, T.Y. and H.L.; validation, T.Y. and Y.Z.; formal analysis, T.Y.; investigation, T.Y. and H.L.; resources, T.Y.; data curation, S.X.; writing—original draft preparation, T.Y. and H.L.; writing—review and editing, T.Y. and Y.Z.; visualization, T.Y. and M.S.; supervision, Y.Z.; project administration, S.X. All authors have read and agreed to the published version of the manuscript.

Funding

This research received no external funding

Notes

The authors declare no competing financial interest.

■ ACKNOWLEDGMENTS

The authors acknowledge the support from the Laboratory of Polymer Matrix Composites, Beihang University.

■ REFERENCES

(1) Ma, X.; Chen, S. a.; Mei, M.; Li, Y.; Li, G.; Hu, H.; He, X.; Qu, X. Microstructure and mechanical behaviors of T700 carbon fiber reinforced C/SiC composites via precursor infiltration and pyrolysis. *Mater. Sci. Eng. A* **2016**, *666*, 238−244.

(2) Wang, M.-l.; Bian, W.-f. The relationship between the mechanical properties and microstructures of carbon fibers. *N. Carbon Mater.* **2020**, *35*, 42−49.

(3) Yang, T.; Zhao, Y.; Chen, W.; Liu, H. Effect of carbon fiber surface microstructure on mechanical properties of CCF800. *J. Mater. Res. Technol.* **2020**, *9*, 8714−8722.

(4) Zhang, S.-j.; Wang, R.-m.; Liao, Y.-q. A comparative study of two kinds of T800 carbon fibers produced by different spinning methods for the production of filament-wound pressure vessels. *N. Carbon Mater.* **2019**, *34*, 578−586.

(5) Duan, S.; Liu, F.; Pettersson, T.; Creighton, C.; Asp, L. E. Determination of transverse and shear moduli of single carbon fibres. *Carbon* **2020**, *158*, 772−782.

(6) Zhang, Y.; Zhang, L.; Guo, L.; Feng, Y.; Liu, G.; Sun, X. Investigation on fatigue performance of T800 composites structural component. *Compos. Struct.* **2018**, *195*, 26−35.

(7) Turkenburg, D. H.; Fischer, H. R. Self-healing mechanism based on dispersed solid particles of various monomeric bismaleimides. *Mater. Today Commun.* **2016**, *8*, 148−155.

(8) Nalwa, H. S.; Suzuki, M.; Takahashi, A.; Kageyama, A.; Nomura, Y.; Honda, Y. High Performance Polyquinoline/Bismaleimide Miscible Blends. *Chem. Mater.* **1998**, *10*, 2462−2469.

(9) Yuan, L.; Gu, A.; Liang, G.; Zhang, Z. Microcapsule-modified bismaleimide (BMI) resins. *Compos. Sci. Technol.* **2008**, *68*, 2107−2113.

(10) Radue, M. S.; Varshney, V.; Baur, J. W.; Roy, A. K.; Odegard, G. M. Molecular Modeling of Cross-Linked Polymers with Complex Cure Pathways: A Case Study of Bismaleimide Resins. *Macromolecules* **2018**, *51*, 1830−1840.

(11) Xu, D.; Cao, Z.; Wang, T.; Zhao, J.; Zhong, J.; Xiong, P.; Wang, J.; Gao, F.; Shen, L. Effect of the Ratio of Acetylacetate Groups on the Properties of a Novel Plant-Based Dual-Cure Coating System. *ACS Omega* **2019**, *4*, 11173−11180.

(12) Lin, Q.; Li, J.; Yang, Y.; Xie, Z. Thermal behavior of coal-tar pitch modified with BMI resin. *J. Anal. Appl. Pyrol.* **2010**, *87*, 29−33.
(13) Qin, H.; Mather, P. T.; Baek, J.-B.; Tan, L.-S. Modification of bisphenol-A based bismaleimide resin (BPA-BMI) with an allyl-terminated hyperbranched polyimide (AT-PAEKI). *Polymer* **2006**, *47*, 2813−2821.
(14) Zhou, J.; Yao, Z.; Zhen, W.; Wei, D.; Li, S. Dielectric and thermal performances of the graphene/bismaleimide/2,2'-diallylbisphenol A composite. *Mater. Lett.* **2014**, *124*, 155−157.
(15) Lin, Q.; Zheng, R.; Tian, P. Preparation and characterization of BMI resin/graphite oxide nanocomposites. *Polym. Test.* **2010**, *29*, 537−543.
(16) Shaoquan, W.; Shangli, D.; Yu, G.; Yungang, S. Thermal ageing effects on mechanical properties and barely visible impact damage behavior of a carbon fiber reinforced bismaleimide composite. *Mater. Des.* **2017**, *115*, 213−223.
(17) Kamiyama, S.; Hirano, Y.; Okada, T.; Ogasawara, T. Lightning strike damage behavior of carbon fiber reinforced epoxy, bismaleimide, and polyetheretherketone composites. *Compos. Sci. Technol.* **2018**, *161*, 107−114.
(18) Yu, Q.; Chen, P.; Wang, L. Degradation in mechanical and physical properties of carbon fiber/bismaleimide composite subjected to proton irradiation in a space environment. *Nucl. Instrum. Methods Phys. Res., Sect. B* **2013**, *298*, 42−46.
(19) Akay, M.; Spratt, G. R.; Meenan, B. The effects of long-term exposure to high temperatures on the ILSS and impact performance of carbon fibre reinforced bismaleimide. *Compos. Sci. Technol.* **2003**, *63*, 1053−1059.
(20) Wang, Q.; Li, X.; Chang, T.; Hu, Q.; Yang, X. Terahertz spectroscopic study of aeronautical composite matrix resins with different dielectric properties. *Optik* **2018**, *168*, 101−111.
(21) Liu, Z.; Hao, A.; Zhang, S.; Dessureault, Y.-S.; Liang, R. Lightweight carbon nanotube surface thermal shielding for carbon fiber/bismaleimide composites. *Carbon* **2019**, *153*, 320−329.
(22) Zhao, Z. J.; Xian, G. J.; Yu, J. G.; Wang, J.; Tong, J. F.; Wei, J. H.; Wang, C. C.; Moreira, P.; Yi, X. S. Development of electrically conductive structural BMI based CFRPs for lightning strike protection. *Compos. Sci. Technol.* **2018**, *167*, 555−562.
(23) Chen, J.; Wang, K.; Zhao, Y. Enhanced interfacial interactions of carbon fiber reinforced PEEK composites by regulating PEI and graphene oxide complex sizing at the interface. *Compos. Sci. Technol.* **2018**, *154*, 175−186.
(24) Chen, Y.; Xu, D.; Zeng, Q.; Liu, S.; Chen, P. Influence of DBD-grafted multi-carboxyl polyurethane on interfacial properties of PBO fibre-reinforced BMI resin composites. *Appl. Surf. Sci.* **2020**, *512*, 145662.
(25) Varshney, V.; Roy, A. K.; Baur, J. W. Modeling the Role of Bulk and Surface Characteristics of Carbon Fiber on Thermal Conductance across the Carbon-Fiber/Matrix Interface. *ACS Appl. Mater. Interfaces* **2015**, *7*, 26674−26683.
(26) Karakassides, A.; Ganguly, A.; Tsirka, K.; Paipetis, A. S.; Papakonstantinou, P. Radially Grown Graphene Nanoflakes on Carbon Fibers as Reinforcing Interface for Polymer Composites. *ACS Appl. Nano Mater.* **2020**, *3*, 2402−2413.
(27) Drakopoulos, S. X.; Psarras, G. C.; Forte, G.; Martin-Fabiani, I.; Ronca, S. Entanglement dynamics in ultra-high molecular weight polyethylene as revealed by dielectric spectroscopy. *Polymer* **2018**, *150*, 35−43.
(28) Lu, B.; Lamnawar, K.; Maazouz, A.; Sudre, G. Critical Role of Interfacial Diffusion and Diffuse Interphases Formed in Multi-Micro-/Nanolayered Polymer Films Based on Poly(vinylidene fluoride) and Poly(methyl methacrylate). *ACS Appl. Mater. Interfaces* **2018**, *10*, 29019−29037.
(29) Wang, Y.; Raman Pillai, S. K.; Che, J.; Chan-Park, M. B. High Interlaminar Shear Strength Enhancement of Carbon Fiber/Epoxy Composite through Fiber- and Matrix-Anchored Carbon Nanotube Networks. *ACS Appl. Mater. Interfaces* **2017**, *9*, 8960−8966.
(30) Zheng, C.; Wang, S.; Liang, S. Interface bonding mechanisms of co-cured damping carbon fiber reinforced epoxy matrix composites. *J. Alloys Compd.* **2020**, *822*, 153739.
(31) Liang, X.; Gao, Y.; Duan, J.; Liu, Z.; Fang, S.; Baughman, R. H.; Jiang, L.; Cheng, Q. Enhancing the strength, toughness, and electrical conductivity of twist-spun carbon nanotube yarns by π bridging. *Carbon* **2019**, *150*, 268−274.
(32) Wu, Y.; Dhamodharan, D.; Wang, Z.; Wang, R.; Wu, L. Effect of electrophoretic deposition followed by solution pre-impregnated surface modified carbon fiber-carbon nanotubes on the mechanical properties of carbon fiber reinforced polycarbonate composites. *Composites, Part B* **2020**, *195*, 108093.
(33) Patnaik, S.; Gangineni, P. K.; Prusty, R. K. Influence of cryogenic temperature on mechanical behavior of graphene carboxyl grafted carbon fiber reinforced polymer composites: An emphasis on concentration of nanofillers. *Compos. Commun.* **2020**, *20*, 100369.
(34) Wang, X.; Huang, Z.; Lai, M.; Jiang, L.; Zhang, Y.; Zhou, H. Highly enhancing the interfacial strength of CF/PEEK composites by introducing PAIK onto diazonium functionalized carbon fibers. *Appl. Surf. Sci.* **2020**, *510*, 145400.
(35) Liu, L.; Jia, C.; He, J.; Zhao, F.; Fan, D.; Xing, L.; Wang, M.; Wang, F.; Jiang, Z.; Huang, Y. Interfacial characterization, control and modification of carbon fiber reinforced polymer composites. *Compos. Sci. Technol.* **2015**, *121*, 56−72.
(36) Wu, Q.; Li, M.; Gu, Y.; Wang, S.; Yao, L.; Zhang, Z. Effect of sizing on interfacial adhesion of commercial high strength carbon fiber-reinforced resin composites. *Polym. Compos.* **2016**, *37*, 254−261.
(37) Tretinnikov, O. N.; Ikada, Y. Dynamic Wetting and Contact Angle Hysteresis of Polymer Surfaces Studied with the Modified Wilhelmy Balance Method. *Langmuir* **1994**, *10*, 1606−1614.
(38) Zhang, X.; Fan, X.; Yan, C.; Li, H.; Zhu, Y.; Li, X.; Yu, L. Interfacial microstructure and properties of carbon fiber composites modified with graphene oxide. *ACS Appl. Mater. Interfaces* **2012**, *4*, 1543−1552.
(39) Sun, P.; Zhao, Y.; Luo, Y.; Sun, L. Effect of temperature and cyclic hygrothermal aging on the interlaminar shear strength of carbon fiber/bismaleimide (BMI) composite. *Mater. Des.* **2011**, *32*, 4341−4347.
(40) Nash, N. H.; Young, T. M.; Stanley, W. F. The reversibility of Mode-I and -II interlaminar fracture toughness after hydrothermal aging of Carbon/Benzoxazine composites with a thermoplastic toughening interlayer. *Compos. Struct.* **2016**, *152*, 558−567.

https://doi.org/10.1021/acsomega.1c01103
ACS Omega 2021, 6, 23028−23037